Longitudinal and transverse electron-nucleus scattering form factors of ^{25}Mg

Anwer A. Al-Sammarraie,[1,2,4,*] Fadhil I. Sharrad,[1,3,4,†] Norhasliza Yusof,[1,4] and Hasan Abu Kassim[1,4]

[1]*Department of Physics, Faculty of Science, University of Malaya, 50603 Kuala Lumpur, Malaysia*

[2]*Department of Chemistry, College of Education, University of Samarra, 34010 Selah Alden, Iraq*

[3]*Department of Physics, College of Science, University of Kerbala, 56001Karbala, Iraq*

[4]*Department of Physics, Quantum Science Centre, Faculty of Science, University of Malaya, 50603 Kuala Lumpur, Malaysia*

(Received 9 May 2015; revised manuscript received 24 June 2015; published 28 September 2015)

The one-body density-matrix elements obtained from the USDA Hamiltonian are used to calculate the electron-nucleus scattering form factors for the ^{25}Mg nucleus. The longitudinal form factor calculations produce good agreements for all states in the first sequence whereas the shell-model predictions show a variation in results for the excitation states in the second sequence. The wave functions of radial single-particle matrix elements have been calculated with the Woods-Saxon, harmonic-oscillator, and Skyrme (Sk42) potentials. The results of the inelastic transverse form factors are in good agreement with the experimental data when using the Sk42 potential whereas the elastic magnetic scattering results show a significant difference in values compared with the experimental data. However the overall shape and other features of the form factors are satisfactory when using the harmonic-oscillator potential. The effective g factors were used as adjustable parameters in the OXBASH code to describe the core-polarization effects in the transverse form factor calculations with the use of a harmonic-oscillator size parameter in the elastic magnetic scattering.

DOI: 10.1103/PhysRevC.92.034327 PACS number(s): 25.30.Bf, 25.30.Dh, 21.60.Cs, 27.30.+t

I. INTRODUCTION

Interest in the rich diversity of physical phenomena underscores the reason for conducting many studies, such as those herein, focusing presently on odd-A magnesium isotopes, the ^{25}Mg nucleus being one of the most important of the Mg nuclides, especially in astrophysics. Many papers have recorded the study of the slow-neutron-capture (s) process, an important source of neutrons within the reaction ^{22}Ne(α,n) ^{25}Mg. This reaction plays an important role during core helium burning, in carbon-shell burning [1–3], and is Mg-Al cycle active in stellar H-shell burning [4]. Recently, the nuclear structure of this isotope has been studied by a number of theoretical methods, all dealing with the Λ hyperon in p orbit [5–7].

The nuclear shell-model codes, such as OXBASH [8], ANTOINE [9], NUSHELL [10], and NUSHELLX [11] are globally used to investigate the structure of nuclei. The essential inputs to most shell-model configuration mixing codes are sets of the single-particle matrix elements (SPEs) and two-body matrix elements (TBMEs). These sets are termed "effective interactions" or "model-space Hamiltonians." The sd model space includes the $0d_{5/2}$, $0d_{3/2}$, and $1s_{1/2}$ valence orbits. For this model space, there are three SPEs and 63 TBMEs which in the mass region of $A = 16$–40 can determine the energies and wave functions for about 10^6 levels. The universal sd (USD) of the Wildenthal interaction Hamiltonian [12] has provided realistic sd-shell wave functions for use in the study of nuclear structure, nuclear spectroscopy, and nuclear astrophysics. Recognizing updates in the data from experiments on sd-shell experimental states, the new sd-shell universal Hamiltonians (USDA and USDB) are refinements in the derivation of the USD Hamiltonian [13]. The new sd-shell effective interactions are based on linear combinations fitted to 608 energy data in sd-shell nuclei ($A = 16$–40) with root-mean-square (rms) deviations of 130 and 170 keV for USDA and USDB, respectively [14,15]. The single-particle energies for the $0d_{3/2}$, $0d_{5/2}$, and $1s_{1/2}$ orbitals are 1.9798, −3.9436, and −3.0612 MeV for the USDA interaction and 2.1117, −3.9257, and −3.2079 MeV for the USDB interaction. The USDA values are close to the renormalized G-matrix values, and although the USDB differs more greatly from the renormalized G-matrix values it nevertheless provides a better fit to the energy data.

High-energy electrons scattering from nuclei represent a powerful tool for studying nuclear structure using the information provided by spectroscopy of the target nucleus. The electron-scattering form factors depend on the momentum transfer, containing information on the spatial structure of the ground states and the excited states, in comparison with the ordinary γ transitions.

Recently, using shell-model calculations, a study has been made of elastic and inelastic electron-nucleus scattering from ^{23}Na, ^{25}Mg, ^{27}Al, and ^{41}Ca nuclei [16]. The one-body density-matrix (OBDM) elements are obtained from the USDA and USDB Hamiltonians. The calculations are conducted using the Michigan three-range Yukawa (CPM3Y) code with and without inclusion of the core-polarization effects. The calculations have shown that the core-polarization effects are essential in obtaining a reasonable description for the form factor results especially for the transverse form factors in ^{25}Mg. The precision of the USDA Hamiltonian for the odd-A magnesium isotopes has been verified by calculating the energy levels, reduced electric quadrupole transition probabilities, and reduced magnetic dipole transition probabilities [17]. The calculations have been performed using the OXBASH code for Windows [8]. Comparison with the experimental data

*anwer_ahmaed@yahoo.com

†fadhil.altaie@gmail.com

shows good accord of the USDA Hamiltonian for the ^{25}Mg results.

In this paper we employ the conservative USDA Hamiltonian to calculate the elastic and inelastic electron-scattering form factors for ^{25}Mg. The aim of present paper is to adopt the USDA wave functions for the zeroth-order wave functions and examine the effects of core polarization by using the effective charges and/or effective g factors as adjustable parameters in the OXBASH calculations. Theoretical calculations of the energy levels and electron-scattering form factors are compared against the experimental data, the transverse elastic and inelastic form factor results are further compared against other theoretical calculations.

II. THEORY

There are two types of electron-scattering form factors: Coulomb or longitudinal $F(C\lambda,q,f,i)$ and transverse with both types of magnetic $F(M\lambda,q,f,i)$ and electric $F(E\lambda,q,f,i)$ where λ is the multipolarity. The total Coulomb $[F_c^2(q,f,i)]$ form factors are given by [18]

$$F_c^2(q,f,i) = \sum_{\lambda} F^2(C\lambda,q,i,f). \tag{1}$$

The total transverse $F_T^2(q,f,i)$ form factors are given by [18]

$$F_T^2(q,f,i) = \sum_{\lambda} [F^2(E\lambda,q,i,f) + F^2(M\lambda,q,i,f)]. \tag{2}$$

Every transverse form factor has two components λ_c and λ_m, arising from the convection currents (due to the orbital motion of the nucleons) and the magnetization currents (due to the intrinsic magnetic moments of the nucleons), respectively [19]. Therefore, we have

$$F(E\lambda,q,f,i) = F(E\lambda_c,q,f,i) + F(E\lambda_m,q,f,i), \tag{3}$$

$$F(M\lambda,q,f,i) = F(M\lambda_c,q,f,i) + F(M\lambda_m,q,f,i). \tag{4}$$

The final form factor expression is given by [18]

$$F^2(X\lambda,q,f,i) = N_p G_{\rm cm}^2(q)\left[\sum_{t_z,x} w_{fs}(X\lambda x,q,f,i,t_z)\right]^2, \tag{5}$$

where $N_p = [\frac{4\pi}{Z^2(2J_i+1)}]$, $G_{\rm cm}$ is the center-of-mass correction which is given as $G_{\rm cm}(q) = e^{(b^2q^2/4A)}$ with b as the oscillator length parameter chosen to reproduce the rms radius of the nucleus, A is the mass number, its value determined from Ref. [18], $b = \sqrt{\frac{41.4\ \text{MeV fm}^2}{\hbar\omega}}$, $\hbar\omega$ is given in Ref. [20], and $\hbar\omega = 45A^{-(1/3)} - 25A^{-(2/3)}$.

The character x specifies the convection (c) and magnetic current (m) contributions for the electric ($X = E$) and magnetic ($X = M$) form factors, and x stands for the single term of Eq. (2) in the case of the Coulomb ($X = C$) form factor. Here $w_{fs}(X\lambda x,q,f,i,t_z)$ are the reduced matrix elements calculated by taking into account the finite size of the nucleons, where t_z is the proton or neutron isospin. These matrix elements can be found from

$$w_{fs}(X\lambda x,q,f,i,t_z) = w(X\lambda x,q,f,i,t_z)\frac{g_{fs}(Xx,q,t_z)}{g(Xx,t_z)}, \tag{6}$$

where $w(X\lambda x,q,f,i,t_z)$ is the point-nucleon reduced matrix elements [18] and $g(Xx,t_z)$ is the free-nucleon g factors, where for $Xx = Mc, Ec$, or C; $g(Xx,t_z) = g_l(t_z)$ and for $Xx = Mm$ or Em; $g(Xx,t_z) = g_s(t_z)$. The parameters $g_{fs}(Xx,q,t_z)$ are the equivalent q-dependent form factors for free nucleons which are found experimentally as in Ref. [21]. The multiparticle form factors $w(X\lambda x,q,f,i,t_z)$ are given in Ref. [18],

$$w(X\lambda,q,f,i,t_z) = \sum_{k,k'} \text{OBDM}(\lambda,k,k'f,i,t_z) w(X\lambda,q,k,k',t_z), \tag{7}$$

where X stands for C, Mc, Mm, Ec, or Em. The sum (k,k') runs over all pairs of single-particle states in the model space whereas OBDM(λ,k,k',f,i,t_z) are the OBDM elements in the isospin formalism. The calculated OBDM values used in this paper are presented in Table I. Here k and k' are the initial- and final-state quantum numbers, and $w(X\lambda,q,k,k',t_z)$ are the reduced single-particle form factors which are given by the integrals of the appropriate multipole operators over the nucleon coordinates $\vec{r}$,

$$w(C\lambda,q,k,k',t_z) = \int \langle k,t_z \| Y^{(\lambda)}(\hat{r}) j_\lambda(qr) \rho_{t_z}(\vec{r}) \| k',t_z\rangle d^3r, \tag{8}$$

$$w(M\lambda c,q,k,k',t_z) = \int \langle k,t_z \| \vec{M}(\lambda,\lambda,q,\vec{r}).\vec{J}_{t_z}(c,\vec{r}) \| k',t_z\rangle d^3r, \tag{9}$$

$$w(M\lambda m,q,k,k',t_z) = \int \langle k,t_z \| \vec{M}(\lambda,\lambda,q,\vec{r}).\vec{J}_{t_z}(m,\vec{r}) \| k',t_z\rangle d^3r, \tag{10}$$

$$w(E\lambda c,q,k,k',t_z) = \frac{1}{q}\int \langle k,t_z \| [\vec{\nabla} \otimes \vec{M}(\lambda,\lambda,q,\vec{r})\vec{J}_{t_z}(c,\vec{r})] \| k',t_z\rangle d^3r, \tag{11}$$

$$w(E\lambda m,q,k,k',t_z) = \frac{1}{q}\int \langle k,t_z \| [\vec{\nabla} \otimes \vec{M}(\lambda,\lambda,q,\vec{r})\vec{J}_{t_z}(m,\vec{r})] \| k',t_z\rangle d^3r. \tag{12}$$

In the calculation of the shell model, it has been assumed that the nucleus consists of a core and valence nucleons. The core is inert, and only the motion of the valence nucleons in the sd shell model space needs to be considered. However, it can be shown theoretically that the effects of the virtual excitations of the nucleons from the core shells into higher orbits are important. One can use the effective charges and g factors to take into account the model-space truncation effects [18]. The effective charges and g factors are often used as an approximation in the renormalization of the single-particle matrix elements in the shell-model calculations. The effective charges are determined empirically in the sd shell by using

TABLE I. The OBDM elements and the single-particle state with $\Delta T = 0$ for each transition studied in this paper.

J_f	n_f	$E_{\text{expt.}}$ (MeV)	E_{Th} (MeV)	ΔJ	$(nlj)_i$	$(nlj)_f$	OBDM	
							Proton	Neutron
5/2	1	0.0	0.0	1	$1d_{5/2}$	$1d_{5/2}$	0.13866	0.83411
					$1d_{5/2}$	$1d_{3/2}$	0.02503	0.06327
					$1d_{3/2}$	$1d_{5/2}$	−0.02503	−0.06327
					$1d_{3/2}$	$1d_{3/2}$	0.03844	0.00256
					$1d_{3/2}$	$2s_{1/2}$	0.03208	−0.00829
					$2s_{1/2}$	$1d_{3/2}$	−0.03208	0.00829
					$2s_{1/2}$	$2s_{1/2}$	−0.00234	0.03378
				3	$1d_{5/2}$	$1d_{5/2}$	0.11539	0.31625
					$1d_{5/2}$	$1d_{3/2}$	0.02090	0.00935
					$1d_{5/2}$	$2s_{1/2}$	−0.01618	−0.03819
					$1d_{3/2}$	$1d_{5/2}$	−0.02090	−0.00935
					$1d_{3/2}$	$1d_{3/2}$	−0.00104	−0.00917
					$2s_{1/2}$	$1d_{5/2}$	−0.01618	−0.03819
				5	$1d_{5/2}$	$1d_{5/2}$	0.01916	0.65290
3/2	1	0.974	1.035	2	$1d_{5/2}$	$1d_{5/2}$	−0.05490	−0.17693
					$1d_{5/2}$	$1d_{3/2}$	−0.06300	−0.08043
					$1d_{5/2}$	$2s_{1/2}$	−0.04014	−0.00405
					$1d_{3/2}$	$1d_{5/2}$	0.07168	−0.24528
					$1d_{3/2}$	$1d_{3/2}$	−0.05922	−0.07005
					$1d_{3/2}$	$2s_{1/2}$	−0.00407	0.01129
					$2s_{1/2}$	$1d_{5/2}$	−0.04798	−0.36788
					$2s_{1/2}$	$1d_{3/2}$	0.00275	0.03094
				4	$1d_{5/2}$	$1d_{5/2}$	0.03222	0.07628
					$1d_{5/2}$	$1d_{3/2}$	0.02903	0.02713
					$1d_{3/2}$	$1d_{5/2}$	−0.04538	−0.21702
7/2	1	1.611	1.739	1	$1d_{5/2}$	$1d_{5/2}$	0.24688	−0.28368
					$1d_{5/2}$	$1d_{3/2}$	0.09438	−0.06034
					$1d_{3/2}$	$1d_{5/2}$	−0.06998	−0.07832
					$1d_{3/2}$	$1d_{3/2}$	0.03737	0.04533
					$1d_{3/2}$	$2s_{1/2}$	0.02945	0.02594
					$2s_{1/2}$	$1d_{3/2}$	−0.01353	−0.07044
					$2s_{1/2}$	$2s_{1/2}$	−0.00876	−0.03507
				2	$1d_{5/2}$	$1d_{5/2}$	0.74614	0.2362
					$1d_{5/2}$	$1d_{3/2}$	0.31902	0.27801
					$1d_{5/2}$	$2s_{1/2}$	0.34663	0.36697
					$1d_{3/2}$	$1d_{5/2}$	−0.30048	−0.32018
					$1d_{3/2}$	$1d_{3/2}$	0.08133	0.08431
					$1d_{3/2}$	$2s_{1/2}$	−0.16429	−0.15971
					$2s_{1/2}$	$1d_{5/2}$	0.55338	0.56743
					$2s_{1/2}$	$1d_{3/2}$	0.21122	0.16991
				3	$1d_{5/2}$	$1d_{5/2}$	−0.0214	−0.24781
					$1d_{5/2}$	$1d_{3/2}$	0.00134	−0.01237
					$1d_{5/2}$	$2s_{1/2}$	0.00967	0.01176
					$1d_{3/2}$	$1d_{5/2}$	−0.00656	−0.00583
					$1d_{3/2}$	$1d_{3/2}$	0.01039	0.0052
					$2s_{1/2}$	$1d_{5/2}$	−0.01446	−0.06678
				4	$1d_{5/2}$	$1d_{5/2}$	0.21688	0.02635
					$1d_{5/2}$	$1d_{3/2}$	−0.00253	0.02692
					$1d_{3/2}$	$1d_{5/2}$	0.01601	−0.05765
5/2	2	1.964	2.034	2	$1d_{5/2}$	$1d_{5/2}$	0.06439	0.07107
					$1d_{5/2}$	$1d_{3/2}$	0.03894	0.08143
					$1d_{5/2}$	$2s_{1/2}$	0.07006	0.02823
					$1d_{3/2}$	$1d_{5/2}$	−0.07208	0.06594
					$1d_{3/2}$	$1d_{3/2}$	0.02994	0.03898
					$1d_{3/2}$	$2s_{1/2}$	−0.02755	−0.03963
					$2s_{1/2}$	$1d_{5/2}$	0.00521	0.40507

TABLE I. (*Continued.*)

J_f	n_f	$E_{\text{expt.}}$ (MeV)	E_{Th} (MeV)	ΔJ	$(nlj)_i$	$(nlj)_f$	OBDM	
							Proton	Neutron
					$2s_{1/2}$	$1d_{3/2}$	−0.01665	0.04167
				4	$1d_{5/2}$	$1d_{5/2}$	−0.05158	0.23973
					$1d_{5/2}$	$1d_{3/2}$	−0.06022	−0.04662
					$1d_{3/2}$	$1d_{5/2}$	0.07529	−0.01297
1/2	2	2.563	2.722	2	$1d_{5/2}$	$1d_{5/2}$	0.1358	0.14057
					$1d_{5/2}$	$1d_{3/2}$	0.07951	0.07879
					$1d_{5/2}$	$2s_{1/2}$	−0.01788	−0.00302
					$1d_{3/2}$	$1d_{5/2}$	−0.12181	−0.45313
					$1d_{3/2}$	$1d_{3/2}$	0.07572	0.10153
					$1d_{3/2}$	$2s_{1/2}$	0.03918	0.03857
					$2s_{1/2}$	$1d_{3/2}$	0.03823	0.22116
					$2s_{1/2}$	$1d_{3/2}$	−0.01951	−0.00515
3/2	2	2.801	2.868	2	$1d_{5/2}$	$1d_{5/2}$	0.12789	0.15314
					$1d_{5/2}$	$1d_{3/2}$	0.04458	0.00389
					$1d_{5/2}$	$2s_{1/2}$	0.04188	0.08456
					$1d_{3/2}$	$1d_{5/2}$	−0.10153	−0.41231
					$1d_{3/2}$	$1d_{3/2}$	0.06317	0.04007
					$1d_{3/2}$	$2s_{1/2}$	0.00449	0.01689
					$2s_{1/2}$	$1d_{5/2}$	0.04939	0.39369
					$2s_{1/2}$	$1d_{3/2}$	−0.03222	−0.06091
				4	$1d_{5/2}$	$1d_{5/2}$	0.01309	0.00108
					$1d_{5/2}$	$1d_{3/2}$	−0.06865	−0.0929
					$1d_{3/2}$	$1d_{5/2}$	0.05403	−0.20064
9/2	1	3.405	3.515	2	$1d_{5/2}$	$1d_{5/2}$	0.57224	0.18925
					$1d_{5/2}$	$1d_{3/2}$	0.25582	0.21305
					$1d_{5/2}$	$2s_{1/2}$	0.08321	0.24093
					$1d_{3/2}$	$1d_{5/2}$	−0.3053	−0.30754
					$1d_{3/2}$	$1d_{3/2}$	0.13028	0.12346
					$1d_{3/2}$	$2s_{1/2}$	−0.09927	−0.09559
					$2s_{1/2}$	$1d_{5/2}$	0.28222	0.29506
					$2s_{1/2}$	$1d_{3/2}$	0.08008	0.05081
				3	$1d_{5/2}$	$1d_{5/2}$	0.13551	−0.2148
					$1d_{5/2}$	$1d_{3/2}$	0.03425	−0.02721
					$1d_{5/2}$	$2s_{1/2}$	−0.04393	0.00217
					$1d_{3/2}$	$1d_{5/2}$	−0.07429	−0.10215
					$1d_{3/2}$	$1d_{3/2}$	−0.00026	−0.01522
					$2s_{1/2}$	$1d_{5/2}$	0.02409	0.09315
				4	$1d_{5/2}$	$1d_{5/2}$	0.26129	0.16461
					$1d_{5/2}$	$1d_{3/2}$	−0.07578	−0.09148
					$1d_{3/2}$	$1d_{5/2}$	0.18501	0.19611
				5	$1d_{5/2}$	$1d_{5/2}$	0.00417	−0.27563
9/2	2	4.059	3.93	2	$1d_{5/2}$	$1d_{5/2}$	0.01042	0.22552
					$1d_{5/2}$	$1d_{3/2}$	0.0091	0.12201
					$1d_{5/2}$	$2s_{1/2}$	0.12893	0.16418
					$1d_{3/2}$	$1d_{5/2}$	−0.22466	−0.25496
					$1d_{3/2}$	$1d_{3/2}$	0.14729	0.14184
					$1d_{3/2}$	$2s_{1/2}$	0.00492	−0.0019
					$2s_{1/2}$	$1d_{5/2}$	0.05706	−0.00568
					$2s_{1/2}$	$1d_{3/2}$	−0.13216	−0.07951
				4	$1d_{5/2}$	$1d_{5/2}$	−0.19956	−0.14192
					$1d_{5/2}$	$1d_{3/2}$	−0.12721	−0.09662
					$1d_{3/2}$	$1d_{5/2}$	0.19026	0.18869
11/2	1	5.251	5.079	4	$1d_{5/2}$	$1d_{5/2}$	−0.14083	−0.02819
					$1d_{5/2}$	$1d_{3/2}$	−0.28082	−0.23595
					$1d_{3/2}$	$1d_{5/2}$	0.4703	0.53665

TABLE II. The effective charges and g factors used in the present paper.

Transition		Factors					
Longitudinal		Effective charges					
		e_p		e_n			
$C2$ [22]		$1.36e$		$0.45e$			
$C4$ [19]		$1.5e$		$0.5e$			
Transverse		Effective charges		g factors			
	$5/2_1^+ \rightarrow 7/2_1^+$	e_p	e_n	$g_s(p)$	$g_s(n)$	$g_l(p)$	$g_l(n)$
	$M1, E2, M3$	$1.36e$	$0.45e$	5.0	-3.5	1.175	-0.106
	$E4, M5$	$1.5e$	$0.5e$	5.586	-3.826	1.0	0.0
Inelastic	$5/2_1^+ \rightarrow 9/2_1^+$						
	$M1, E2, M3$	$1.36e$	0.45e	5.0	-3.5	1.175	-0.106
	$E4$	$1.5e$	$0.5e$	5.586	-3.826	1.0	0.0
	$M5$	$1.5e$	$0.5e$	5.586	-5.5	1.0	0.0
Elastic	$5/2_1^+ \rightarrow 5/2_1^+$						
	$M1$	$1.36e$	$0.45e$	5.0	-3.3	1.175	-0.16
	$M3$	$1.5e$	$0.5e$	5.5	-3.5	1.175	-0.106
	$M5$	$1.5e$	$0.5e$	5.0	-3.7	1.175	-0.106

the electrical transition ($E2$ and $E4$) matrix elements which are found from the values of the observable $B(E2)$ and $B(E4)$ values [19]. The g factors are fairly well described with the experimental magnetic moments in the sd-shell model predictions. The values are determined by using the least-squares fits to the experimental measurements [22]. The values of the effective charges and g factors which are used in this paper are listed in Table II.

III. RESULTS AND DISCUSSION

A. Energy levels and transition probabilities

The energy levels have been calculated using USDA interaction for ^{25}Mg. The calculated results are successful in predicting the first, second, and third sequences with fractional occupancy numbers for ^{25}Mg as presented in Table III. In the three sequences of $J \leqslant 13/2^+$ with energies up to 10 MeV,

TABLE III. Comparison between the calculated energy levels and the experimental data [23,24] with fractional occupancy for ^{25}Mg.

J^π	Energy (MeV)		p-fractional occupancy			n-fractional occupancy		
	Expt.	USDA	$0d_{3/2}$	$0d_{5/2}$	$1s_{1/2}$	$0d_{3/2}$	$0d_{5/2}$	$1s_{1/2}$
$5/2_1^+$	0.000	0.000	0.130925	0.517733	0.185	0.124575	0.680067	0.21065
$1/2_1^+$	0.585	0.626	0.118725	0.509317	0.2346	0.15705	0.573183	0.4664
$3/2_1^+$	0.974	1.035	0.113625	0.510567	0.24105	0.21405	0.583933	0.3201
$7/2_1^+$	1.611	1.739	0.1196	0.5035	0.2503	0.1265	0.660867	0.26445
$9/2_1^+$	3.405	3.515	0.1347	0.505933	0.21275	0.140725	0.65655	0.24885
$11/2_1^+$	5.251	5.079	0.165425	0.484033	0.217	0.17865	0.640233	0.22195
$13/2_1^+$	5.461	5.529	0.059375	0.588533	0.11565	0.10455	0.714567	0.1472
$15/2_1^+$	9.947	9.491	0.106925	0.5264	0.20695	0.11885	0.652533	0.3047
$5/2_2^+$	1.964	2.034	0.1154	0.49665	0.27925	0.14805	0.55355	0.54325
$1/2_2^+$	2.563	2.722	0.13415	0.50595	0.21385	0.278825	0.554083	0.2801
$7/2_2^+$	2.737	2.802	0.11615	0.512817	0.2293	0.23715	0.587567	0.263
$3/2_2^+$	2.801	2.868	0.127525	0.49515	0.2595	0.220175	0.55845	0.3843
$9/2_2^+$	4.059	3.93	0.139125	0.4703	0.31085	0.154575	0.6327	0.29275
$11/2_2^+$	5.533	5.709	0.098675	0.50215	0.29625	0.165825	0.624867	0.29375
$13/2_2^+$	7.551	7.44	0.1632	0.482067	0.2274	0.16785	0.650433	0.213
$15/2_2^+$	10.653	9.721	0.138725	0.53515	0.1171	0.164575	0.643417	0.2406
$5/2_3^+$	3.907	4.022	0.1384	0.48735	0.26115	0.24505	0.578033	0.2758
$3/2_3^+$	4.359	4.395	0.146925	0.465767	0.30885	0.26855	0.5154	0.41675
$9/2_3^+$	4.711	4.771	0.11435	0.488067	0.30705	0.156675	0.532917	0.5879
$7/2_3^+$	5.012	4.965	0.1324	0.493167	0.2557	0.194975	0.572717	0.39185
$1/2_3^+$	5.474	5.462	0.147725	0.49795	0.2107	0.1732	0.607683	0.33055
$11/2_3^+$	6.04	6.067	0.114675	0.5044	0.25745	0.16505	0.6199	0.3102
$13/2_3^+$	8.076	8.059	0.131875	0.465083	0.341	0.160875	0.5683	0.47335

the excited states in the USDA calculations are in good agreement with the experimental data [23,24] for the ^{25}Mg spectrum. The agreement between the theoretical excited states and the experimental data indicate a set of good wave functions that are capable of describing the behavior of this nucleus. This conclusion is evidenced by the calculations of the reduced transition probabilities values illustrated in Table III in Ref. [17]. Furthermore, $0d_{5/2}$ has contributed significantly in the calculations.

B. Longitudinal form factors

Calculation of the form factor values depends on the OBDM elements as one can see from Eq. (7). As such, the form factors represent a real assessment for the OBDM elements as predicted using the USDA Hamiltonian.

In this paper, the longitudinal form factors have been calculated for all the available experimental transition data from the ground state to the different excited states in the first and second sequences. Three types of potentials have been used, and all parameters used for these potentials are listed in Table IV. The effective charges and OBDM for the $C2$ and $C4$ form factors are presented in Tables I and II, respectively.

Calculation has been performed for $q \leqslant 3\,\mathrm{fm}^{-1}$ in order to show a wide range of theoretical values. Three types of potentials: the harmonic-oscillator, the Woods-Saxon, and the Skyrme interactions have been used for all the assigned transitions in seeking to investigate which interaction can best estimate the experimental values. Our calculations show as will be illustrated later in Figs. 1–8 that the three potentials produced convergent theoretical values with a simple preference for one of these potentials in a specific range of q values.

Reference [25] showed the experimental values for the electron-scattering longitudinal form factors for the transition from the ground state ($J^\pi = 5/2^+$) to the excited state with $J^\pi = 3/2^+$ at an energy of 0.974 MeV in the momentum transfer range of 0.3–1.15 fm^{-1}. According to the multipolarity relation,

$$|J_i - J_f| \leqslant \lambda \leqslant J_i + J_f, \tag{13}$$

where J_i and J_f are the initial and final total angular momenta, respectively, and there are two types of transitions $C2$ and $C4$ for this case. The theoretical and experimental results are illustrated in Fig. 1. The two types of transitions are shown in Fig. 1(a) using the Woods-Saxon potential, whereas Fig. 1(b) shows that the three potentials provide good agreement with the available experimental data.

TABLE IV. The Woods-Saxon, harmonic-oscillator, and Sk42 Skyrme parameter sets [26].

Potential	Parameters	
Woods-Saxon	V_0 central depth (p/n)	52.425 MeV
	V_1	−27.1713 MeV
	r_0, r_{so}	1.263 fm
	a_0, a_{so}	0.7150 fm
	V_{so}	6.0 MeV
	r_c	1.2 fm
Harmonic oscillator	b	Inelastic 1.8245 fm
		Elastic 1.630 fm
Sk42	t_0	−2885.239
	t_1	302.733
	t_2	−323.419
	t_3	18237.492
	Skw$_0$	162.726
	Ska	0.167
	Skx0	0.137
	Skx1	−0.255
	Skx2	−0.607
	Skx3	0.054
	t_s	76.936
	t_v	77.744

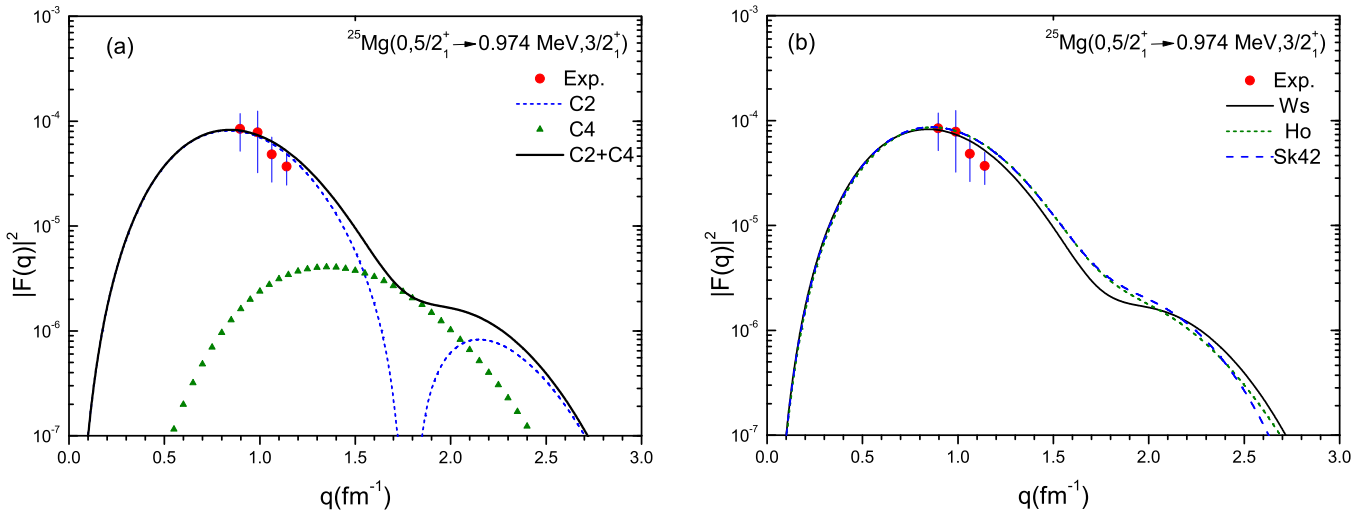

FIG. 1. (Color online) (a) Longitudinal $C2$ and $C4$ electron-scattering form factors for the $5/2^+_1 \rightarrow 3/2^+_1$ transition in ^{25}Mg obtained using the Woods-Saxon potential and USDA Hamiltonian. (b) The total longitudinal form factor obtained by the three potentials. The experimental data are taken from Ref. [25].

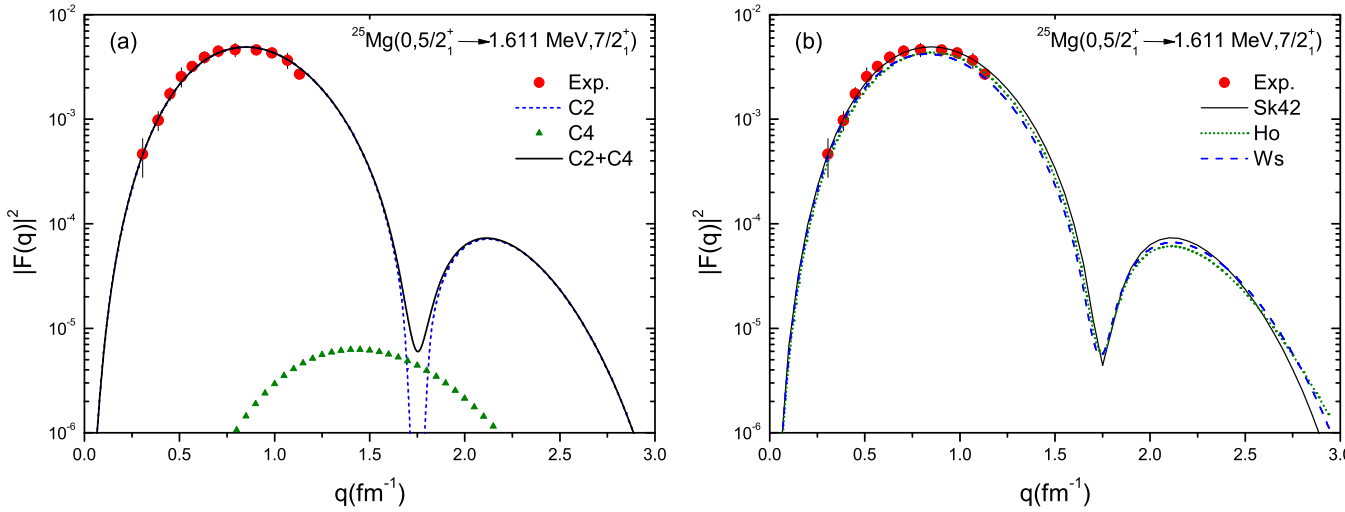

FIG. 2. (Color online) (a) Longitudinal $C2$ and $C4$ electron-scattering form factors for the $5/2^+_1 \rightarrow 7/2^+_1$ transition in ^{25}Mg obtained using the Sk42 potential and USDA Hamiltonian. (b) The total longitudinal form factor obtained by the three potentials. The experimental data are taken from Ref. [27].

Figure 2(a) shows the longitudinal $C2$ and $C4$ form factors for the transition from the ground state to the first $J = 7/2^+$ at an energy of 1.611 MeV. The theoretical and experimental [25] results are in good agreement.

The theoretical values are obtained by using the USDA Hamiltonian and Skyrme interaction potential Sk42 [26]. In this transition, $C4$ has a small contribution to the total form factor whereas $C2$ is dominant for over all q's. Comparison between the three potentials is shown in Fig. 2(b).

Comparison between the theoretical and experimental data [25] $C2$ and $C4$ form factors for the transition $5/2^+_1 \rightarrow 5/2^+_2$ is shown in Fig. 3. Obviously, the experimental measurements have been performed in the area of dominance of $C2$. The $C2$ curve shows acceptable agreement with the experimental data especially when the experimental errors are taken into account. On the other hand, $C4$ is dominant within the range of $q > 1.5\,\mathrm{fm}^{-1}$ as found in the transition $5/2^+_1 \rightarrow 3/2^+_1$ (Fig. 1). Comparison between the three potentials is shown in Fig. 3(b).

According to the multipolarity relation (13), $C2$ is the only allowed electrical transition when ^{25}Mg is excited from the ground state to the excited state with $J = 1/2^+_2$ at an energy of 2.563 MeV. The theoretical results obtained when the Sk42 potential is used are shown in Fig. 4(a) and is shown for the three potentials in Fig. 4(b).

In Fig. 5, the theoretical $C2$ and $C4$ form factors are seen to be in good agreement with the experimental data for q values ranging from 0.5 to 1.0 fm^{-1} when the ^{25}Mg nucleus is excited from the ground state to the excited state of $J = 3/2^+_2$ at an energy of 2.801 MeV. In this transition, the theoretical calculations show a predominance of $C4$ for the limited range

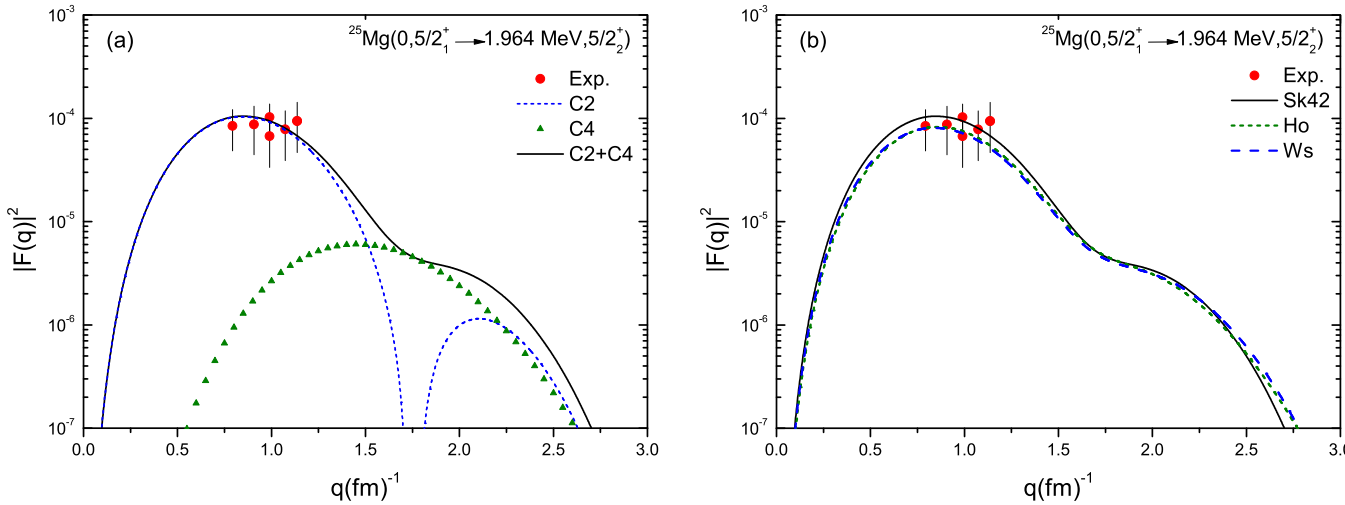

FIG. 3. (Color online) (a) Longitudinal $C2$ and $C4$ electron-scattering form factors for the $5/2^+_1 \rightarrow 5/2^+_2$ transition in ^{25}Mg obtained using the Sk42 potential and USDA Hamiltonian. (b) The total longitudinal form factor obtained by the three potentials. The experimental data are taken from Ref. [25].

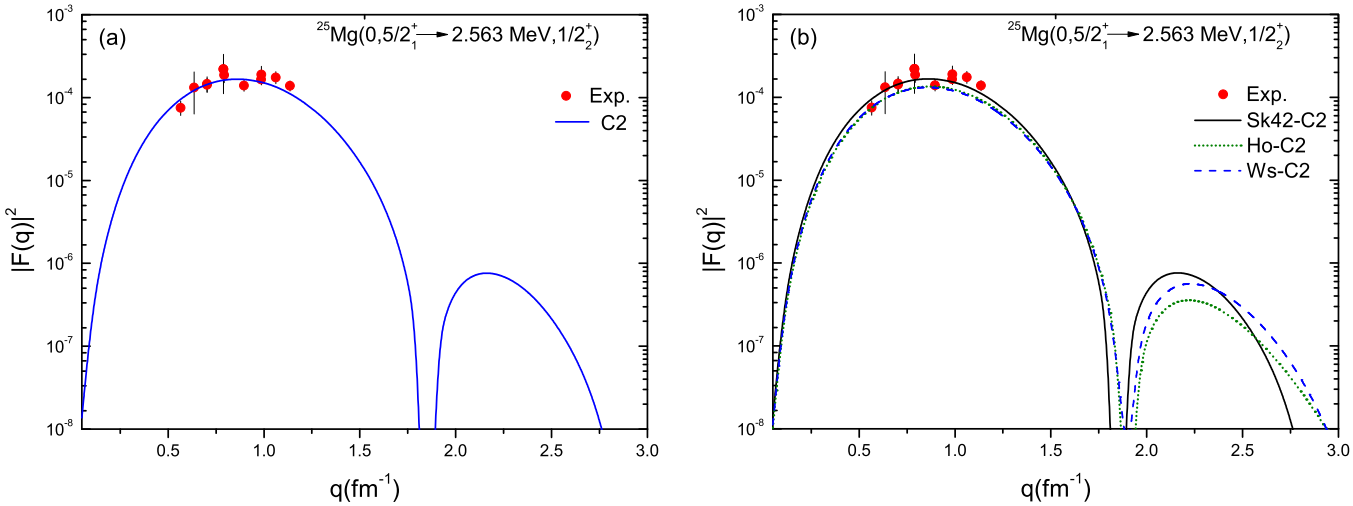

FIG. 4. (Color online) (a) Longitudinal $C2$ electron-scattering form factors for the $5/2^+_1 \rightarrow 1/2^+_2$ transition in ^{25}Mg obtained using the Sk42 potential and USDA Hamiltonian. (b) The total longitudinal form factor obtained using the three potentials. The experimental data are taken from Ref. [25].

of q that lies between 1.7 and 1.8 fm^{-1} with a clear dominance of $C2$ for the rest of the q values.

Our calculations show good accuracy in the description of the longitudinal form factors $C2$ and $C4$ for the transition $5/2^+_1 \rightarrow 9/2^+_1$ at an energy of 3.405 MeV as shown in Fig. 6(a). Comparison with the experimental data [25] indicates that $C2$ has the dominant contribution for most of the q values in this transition; in contrast the $C4$ contribution is limited to $1.8 < q < 1.9$ fm^{-1}. Comparison between the three potentials is shown in Fig. 6(b). From this figure, all potentials are seen to be in good agreement with the experimental data.

The theoretical $C2$ and $C4$ values are lower than the experimental data in the transition $5/2^+_1 \rightarrow 9/2^+_2$ with the excited energy of 4.059 MeV as shown in Fig. 7(a). The total form factor calculation using the three potentials is shown in Fig. 7(b). None of the three potentials do a good job in describing the data for the transition shown in Fig. 7.

The last available experimental longitudinal transition is $5/2^+_1 \rightarrow 11/2^+_1$ with an excited energy of 5.252 MeV. When applying the selection rule Eq. (13), we find that $C4$ is the only allowed transition. The calculation obtained using USDA produces results in good agreement with the experimental data for this excitation for all potentials as one can see in Fig. 8(b).

C. Transverse form factors

The general formula used to calculate the transverse form factor is given in Eq. (2) and includes two parts: magnetic and electric transverse form factors. As such, we have mixed multipolarities for every excitation in the odd nucleus according to the selection rule Eq. (13).

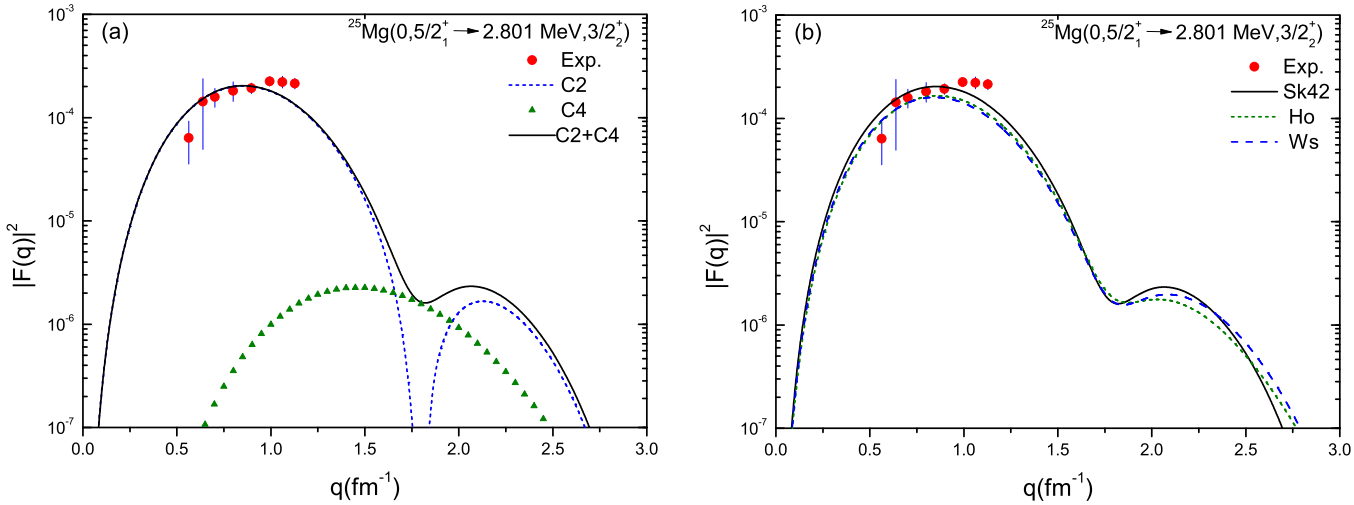

FIG. 5. (Color online) (a) Longitudinal $C2$ and $C4$ electron-scattering form factors for the $5/2^+_1 \rightarrow 3/2^+_2$ transition in ^{25}Mg obtained using the Sk42 potential and USDA Hamiltonian. (b) The total longitudinal form factor obtained by the three potentials. The experimental data are taken from Ref. [25].

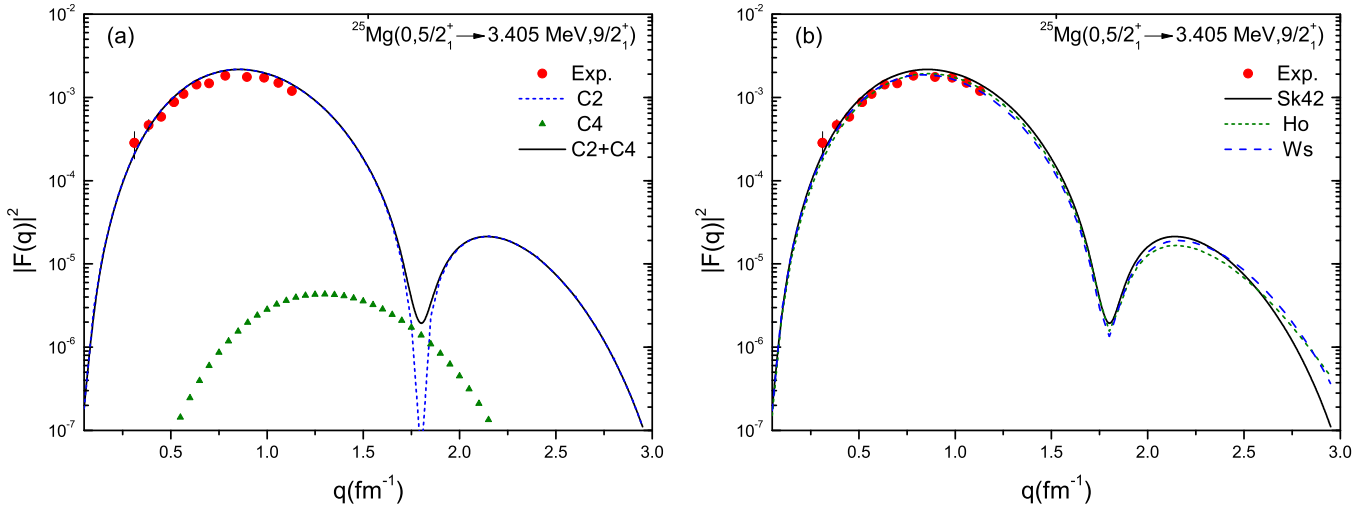

FIG. 6. (Color online) (a) Longitudinal $C2$ and $C4$ electron-scattering form factors for the $5/2^+_1 \rightarrow 9/2^+_1$ transition in ^{25}Mg obtained using the Sk42 potential and USDA Hamiltonian. (b) The total longitudinal form factor obtained by three potentials. The experimental data are taken from Ref. [27].

The electron excites the ^{25}Mg nucleus from the ground state to the $7/2^+_1$ state with the excitation energy of 1.698 MeV [28]. The total transverse form factor for this transition has mixed multipolarities as shown in Fig. 9(a). The theoretical individual multipoles are shown in the same figure. The calculated individual multipoles values are obtained by using the USDA and Sk42 potentials for OXBASH. The new g-factor values [$g_s(p) = 5.0$, $g_s(n) = -3.5$, and $g_l(n) = -0.106$] [22] are used in the $M1$ and $M3$ magnetic transition calculations, and the free-nucleon g factors are used for $M5$. The new effective charges ($e_p = 1.36$ and $e_n = 0.45$) are used in the $M1$ and $E2$ calculations whereas $e_p = 1.5$ and $e_n = 0.5$ [19] are used for the $M3$, $E4$, and $M5$ transitions. In Fig. 9(a), the curves of $M1$ and $M3$ are cut out for high-q values for more obvious viewing, and the values are taken into consideration in the total range from $0 < q < 3\,\mathrm{fm}^{-1}$.

The main contribution in most of the regions of q comes from $M1$ and $M5$. $M1$ has the dominant contribution in the region between 0 and $1.05\,\mathrm{fm}^{-1}$, and $M5$ has the dominant contribution in the range of momentum transfer from 1.1 to $3.0\,\mathrm{fm}^{-1}$. The total transverse form factor [shown as a solid curve in Fig. 9(a)] is in good agreement with the available experimental data.

In regard to comparison between the present paper and the previous work [16], Fig. 9(b) shows an approximately similar individual dominant contribution for every multipole with the remarkable agreement for the OXBASH data in the region of $q < 1.75\,\mathrm{fm}^{-1}$. The total transverse form factor from

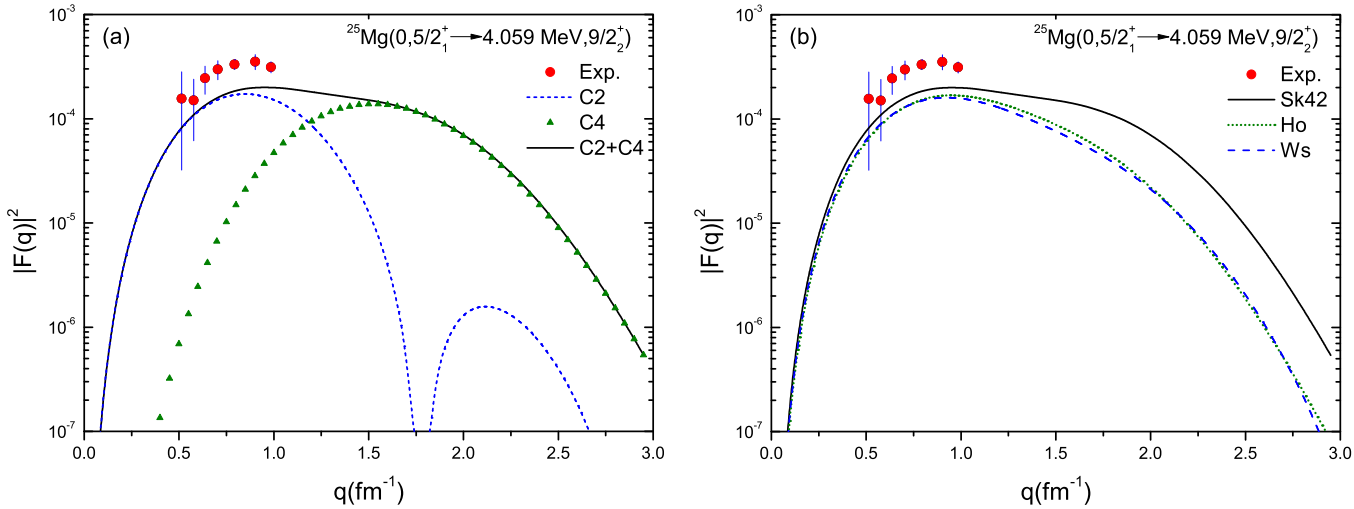

FIG. 7. (Color online) (a) Longitudinal $C2$ and $C4$ electron-scattering form factors for the $5/2^+_1 \rightarrow 9/2^+_2$ transition in ^{25}Mg obtained using the Sk42 potential and USDA Hamiltonian. (b) The total longitudinal form factor obtained by the three potentials. The experimental data are taken from Ref. [25].

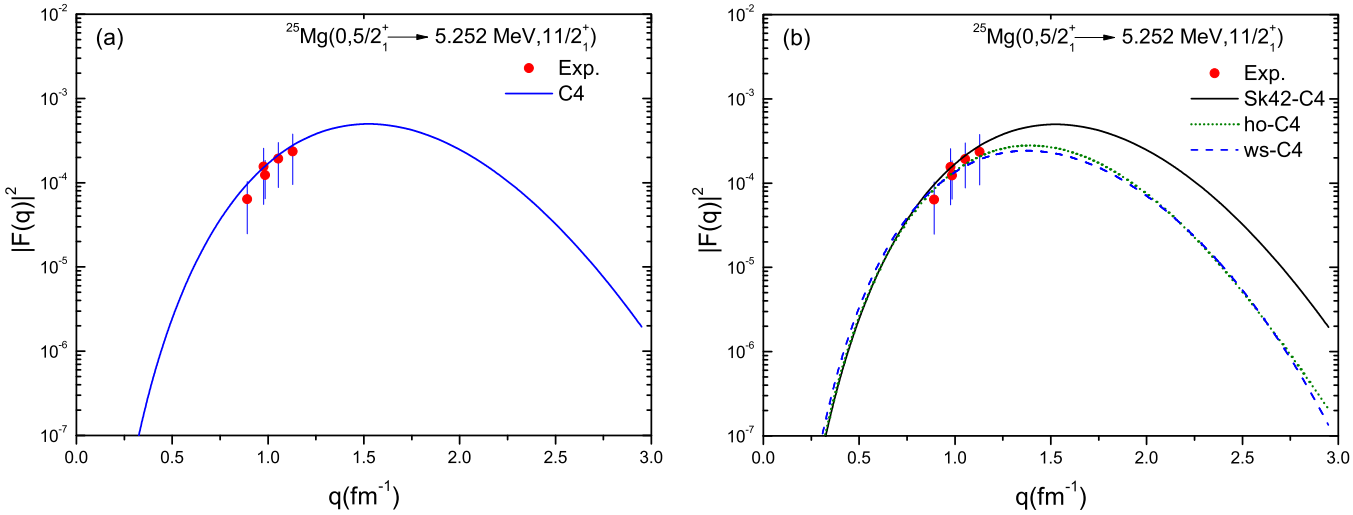

FIG. 8. (Color online) (a) Longitudinal $C2$ and $C4$ electron-scattering form factors for the $5/2^+_1 \rightarrow 11/2^+_1$ transition in ^{25}Mg obtained using the Sk42 potential and USDA Hamiltonian. (b) The total longitudinal form factor obtained by the three potentials. The experimental data are taken from Ref. [25].

the CPM3Y code is close to the experimental data of the sum of $M1 + E2 + M3 + M5$ although the OXBASH calculations contain all the allowed multipolarities $M1 + E2 + M3 + E4 + M5$ for this transition. Agreements in the data shown in Fig. 9(a) indicate that use of the effective charges and effective g factors is a good assignment in describing the core-polarization effects.

The OXBASH code is used to calculate the transverse form factor for the transition $5/2^+_1 \rightarrow 9/2^+_1$ by employing the USDA effective interaction and the Sk42 potential. The individual multipoles of $E2$, $M3$, $E4$, and $M5$ are shown in Fig. 10(a) with the total transverse form factor ($E2 + M3 + E4 + M5$) shown as a solid curve. From comparison with the experimental data [28], the theoretical results (for the total transverse form factor) are less than that of the experimental data. On the other hand, we find that the results of the CPM3Y code ($E2 + M3 + M5$), shown in Fig. 10(b), overestimate the experimental data when the same OBDM elements obtained from USDA are used [16].

We can analyze this case as follows: The difference between OXBASH and CPM3Y results indicates the presence of significant core-polarization effects in this excitation. We have mixed multipolarities of four types: $E2$, $M3$, $E4$, and $E5$. The electrical multipolarities $E2$ and $E4$ show good agreement with the longitudinal transition as shown in Fig. 6(a). This means that it is appropriate to use the effective charges and effective g factors to describe the core-polarization effects for this electrical multipolarity transition. The individual multipole $M3$ is sensitive to the experimental data and describes it very well in the momentum transfer range of $1.25 < q < 1.6\,\mathrm{fm}^{-1}$. $M5$ is the residual multipole which has the dominant contribution in the experimental data range.

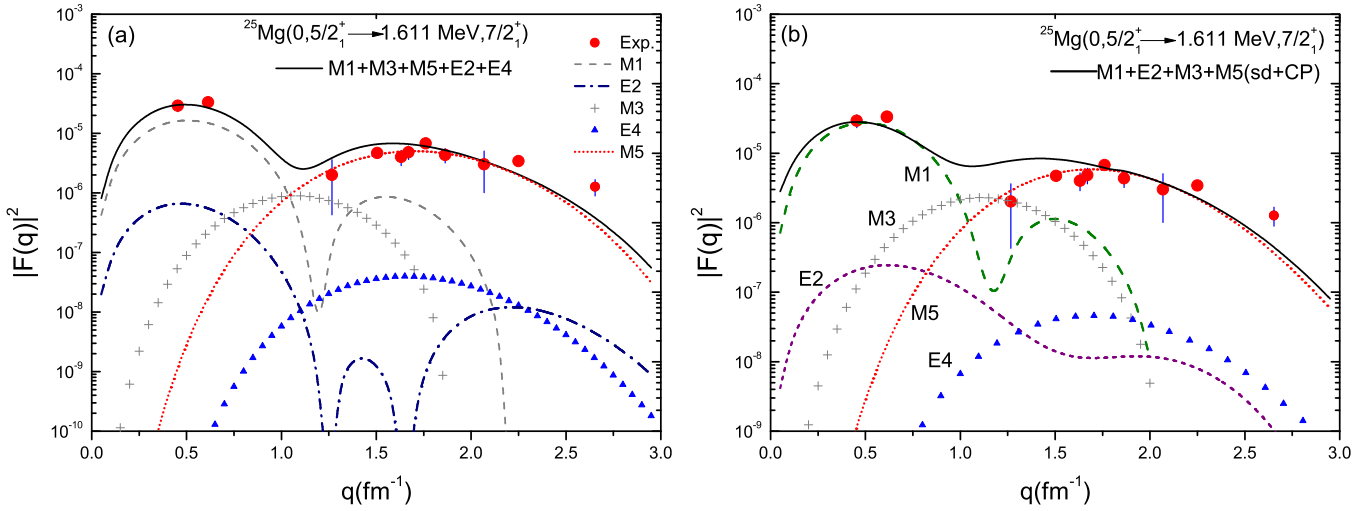

FIG. 9. (Color online) Transverse $M1$, $E2$, $M3$, $E4$, and $M5$ electron-scattering form factors for the $5/2^+_1 \rightarrow 7/2^+_1$ transition in ^{25}Mg: (a) present paper, obtained using both the Sk42 potential and the USDA Hamiltonian in the OXBASH code and (b) Ref. [16]. The experimental data are taken from Ref. [28].

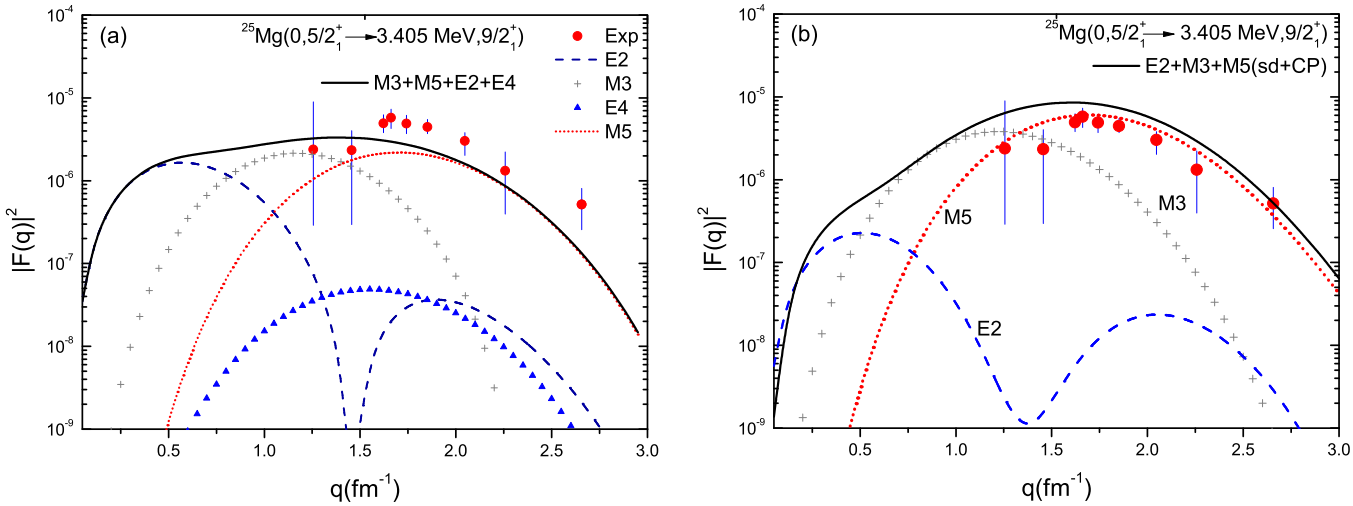

FIG. 10. (Color online) Transverse $M1$, $E2$, $M3$, $E4$, and $M5$ electron-scattering form factors for the $5/2^+_1 \rightarrow 9/2^+_1$ transition in ^{25}Mg: (a) present paper, obtained using both the Sk42 potential and the USDA Hamiltonian in the OXBASH code and (b) Ref. [16]. The experimental data are taken from Ref. [28].

Compared with the CPM3Y results, we attribute the differences to the significant core-polarization effects in the $M5$ excitation. To investigate this effect, we have changed the free-space values for the $M5$ excitation which are in this case the g factors values. In Fig. 10(a), we use the following free-nucleon g-factor values: $g_s(p) = 5.586$, $g_s(n) = -3.826$, $g_l(p) = 1.0$, and $g_l(n) = 0$. The calculations are individually achieved with different values for every g component, and we find that the $M5$ form factor has higher sensitivity to $g_s(n)$ than to the other components $g_s(p)$, $g_l(p)$, and $g_l(n)$. We have identified the value of $g_s(n) = -5.5$ and an increase of 43% in the absolute $g_s(n)$ value as the best value used to obtain $M5$ and the total form factor in order to be consistent with the experimental data for the transition $5/2^+_1 \rightarrow 9/2^+_1$ as shown in Fig. 11.

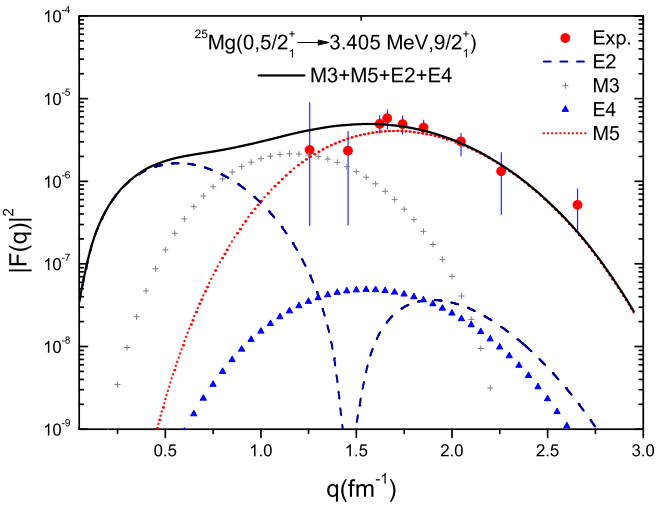

FIG. 11. (Color online) Transverse $E2$, $M3$, $E4$, and $M5$ electron-scattering form factors for the $5/2^+_1 \rightarrow 9/2^+_1$ transition in ^{25}Mg obtained with the Sk42 potential, the USDA Hamiltonian using the OXBASH code, and the free-nucleon g factors with $g_s(n) = -5.5$ in the $M5$ calculation. The experimental data are taken from Ref. [28].

D. Magnetic transverse elastic form factors

In the present paper, we have used the plane-wave Born approximation to calculate the magnetic elastic-scattering form factors and compared with the experimental data. Experiments have been performed by Euteneuer *et al.* [29] for a momentum transfer range from 0.19 to 2.56 fm^{-1}. Euteneuer *et al.* [29] have examined the effective momentum transfer values $q_{\rm eff}$ defined by the equation [18],

$$q_{\rm eff}(\text{magnetic multipoles}) = q_0\left(\frac{1+1.2Ze^2}{E_eR}\right),$$
$$R^2 = \frac{5}{3}\langle r^2\rangle, \tag{14}$$

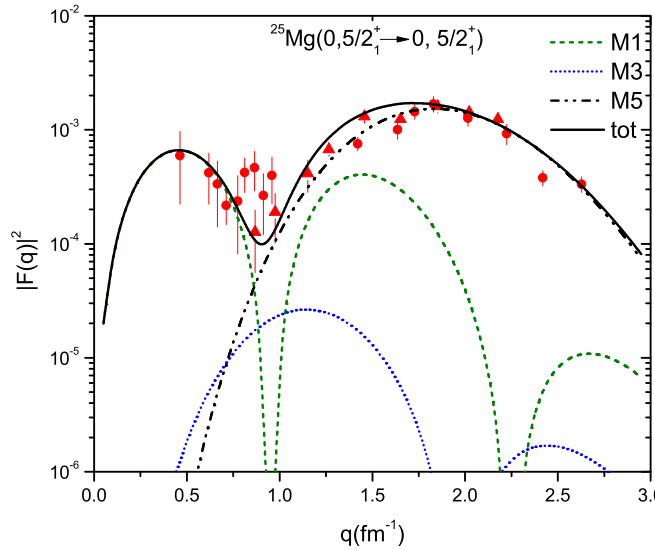

FIG. 12. (Color online) Elastic magnetic electron-scattering form factors in ^{25}Mg. The theoretical results have been multiplied by a factor of 170. The experimental data are taken from Ref. [29] (full circle) and from Ref. [30] (full triangle).

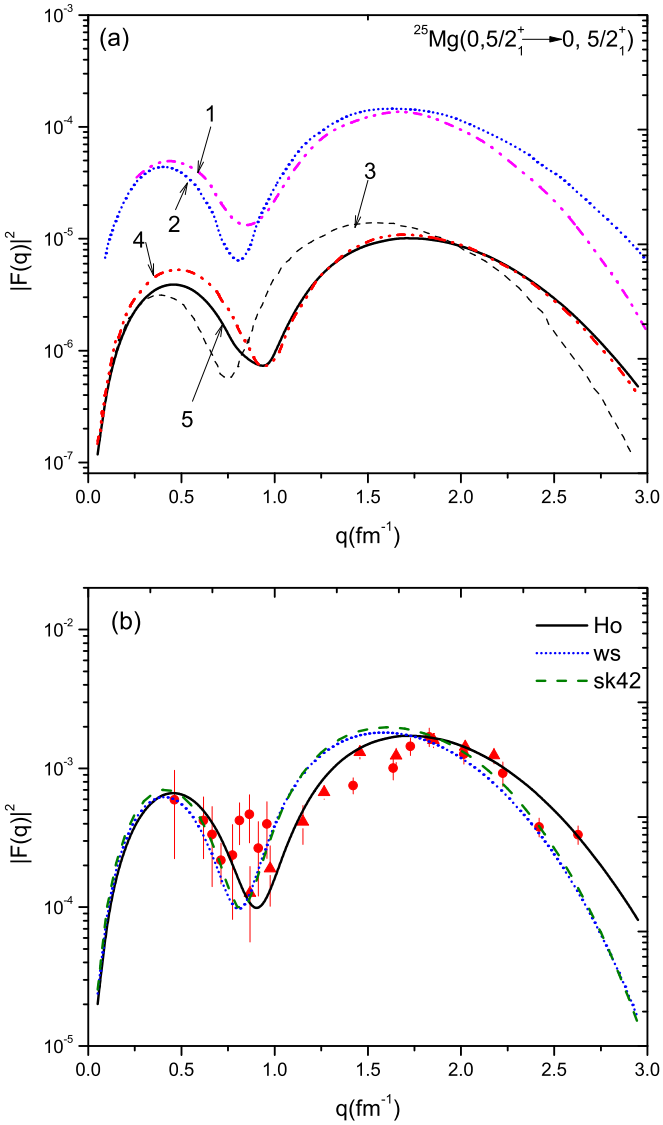

FIG. 13. (Color online) (a) The shell-model prediction of the total magnetic elastic-scattering form factors in this paper (curve 5) compared to the results of the shell-model using the matrix elements of the Brown and Wildenthal and Woods-Saxon radial wave functions (curve 1) [31] using the Nilsson model (curve 2) [31], the shell-model using the *cwc* interaction, and the Woods-Saxon wave functions (curve 3) [32], and the shell-model with the core-polarization effects with the harmonic-oscillator potential reduces the $b_{\rm rms}$ value by 5% (curve 4) [33]. (b) The total magnetic elastic-scattering form factors obtained by the three potentials.

where R is the hard-sphere radius, r is the rms charge radius, Z is the atomic number of the target nucleus, and E_e is the electron energy, finding excellent overlap between distorted-wave and plane-wave form factors for all multipoles. Also the magnetic elastic-scattering form factor for ^{25}Mg has been measured by York and Peterson [30] for q from 0.8 to 2.2 fm^{-1}.

The form factors calculated with the *sd* shell model shown in Fig. 12 depend on the single-particle wave functions of the harmonic-oscillator potential with radial size parameter $b = 1.63$ fm. The OBDM elements, the effective charges,

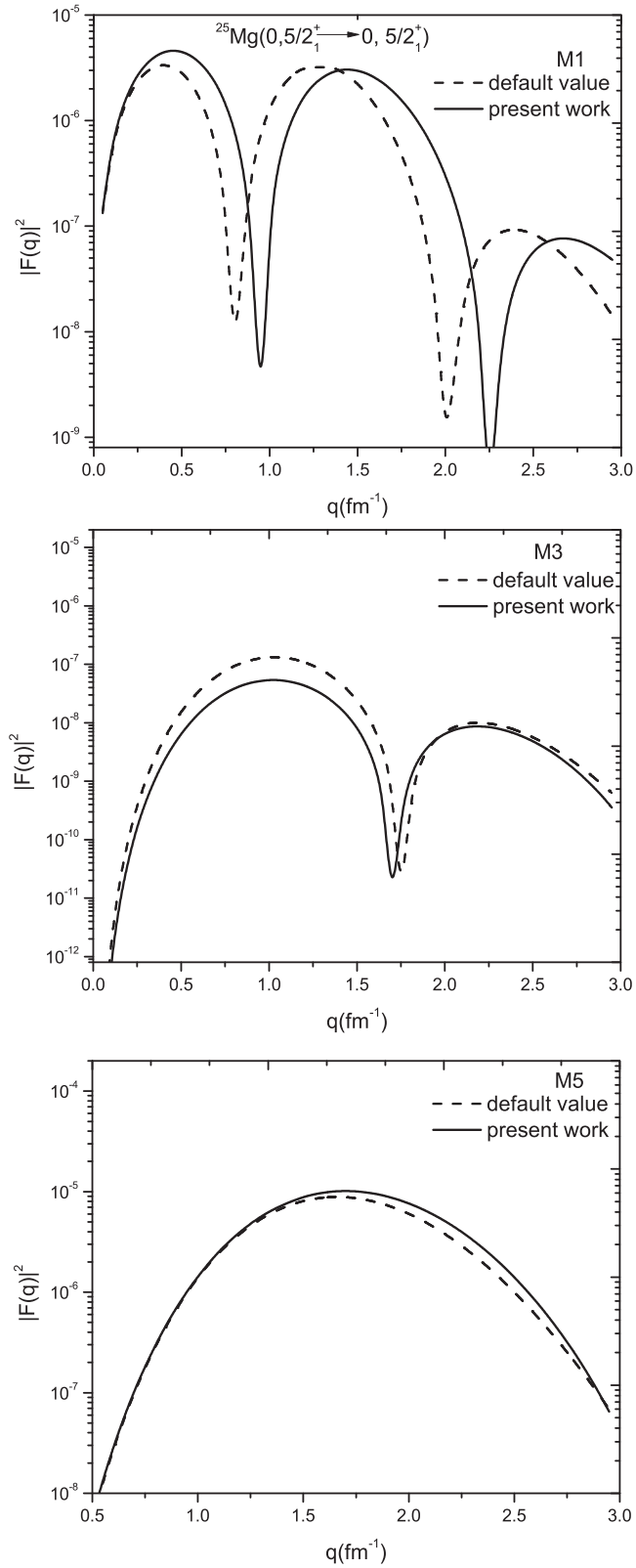

FIG. 14. The individual $M1$, $M3$, and $M5$ form factors. The dashed curve is calculated using the shell-model with the $b = b_{\rm rms}$ harmonic-oscillator potential and the g-factor values taken from USDA(6) [22]. The solid curve is calculated using the shell-model with the $b = 1.63$ harmonic-oscillator potential and the g-factor values given in Table II.

and g factors are presented in Tables I and II, respectively. A significant difference has been found in values between the original experimental data [29,30] and theoretical results, which involved multiplying the theoretical data by a factor of 170, carried out in order to match with the experimental data. In many of the previous studies, the corrections were needed in order to make the data more reliable. Donnelly [31] has mentioned that the experimental data [29] were obtained at $\theta = 160^{\circ}$, including the statistical and systematical errors. Donnelly [31] reduced the experimental data of Refs. [29,30] with a factor of $\approx 8 \times 10^{-2}$, whereas Singhal *et al.* [32] and Radhi *et al.* [33] reduced the experimental data with $\approx 5 \times 10^{-3}$. The magnetic elastic-scattering form factors obtained in this paper are very close to the shell-model calculations from Refs. [32,33], whereas the predictions of Nilsson and the shell models from Ref. [31] were higher as we can see in Fig. 13(a). The overall shape and other features of the form factors are similar to the experimental data. The higher contribution in the first lobe of $M1$ appears to match the experimental values at $q \approx 0.45\,\mathrm{fm}^{-1}$, and the low point at $q \approx 0.9\,\mathrm{fm}^{-1}$ is more compatible compared to the other potentials as we can see in Fig. 13(b). Additionally, as one can see in Fig. 13(b), the total form factors obtained from the single-particle wave functions of the harmonic-oscillator potential show good agreement with the experimental data in the region of $q \approx 0.45$ to $q \approx 1.8\,\mathrm{fm}^{-1}$ compared with the values calculated by using the Sk42 and Woods-Saxon potentials.

The g factor and the radial size parameter values used in this paper (see Tables I and II) give the best overall agreement between the calculated and the experimental form factors. The effects of changing these values in all multipolarities are presented individually in Fig. 14. For $M1$ the identified orbital and spin g-factor values of the neutron result in an increase in the first lobe and a decrease in the second lobe and changing of the b value, shifting $M1$ to the higher q value. This modification has produced more theoretical values which agree with the experimental data within the range of $q < 1\,\mathrm{fm}^{-1}$. This behavior is similar to that found in adding the core-polarization effects [33]. The opposite behavior of the $M3$ values makes the theoretical results more appropriate in the lower range. Using the size parameter decreased by 10% from the b_{rms} value moves the maxima of the $M5$ form factors to larger momentum transfer, leading to a better fit for $q > 1.7\,\mathrm{fm}^{-1}$ as shown in Fig. 14 by the solid curve.

IV. CONCLUSION

The transition one-body density matrices predicted by employing the USDA Hamiltonian are used to calculate the electron-scattering form factors of the ^{25}Mg isotopes. The results of the longitudinal form factors $C2$ and $C4$ reproduce well the data for low-momentum transfer $q < 1.2\,\mathrm{fm}^{-1}$ according to the available experimental data. Our calculations have shown a clear significance of the $C4$ transition especially for the region of $q > 1.7\,\mathrm{fm}^{-1}$.

The longitudinal form factor results show a reasonable accuracy of the USDA in the excitations to the first sequence states of the ^{25}Mg, and this accuracy varies in the second sequence according to the energy of the excited state in inverse proportion. The harmonic-oscillator, Woods-Saxon, and Skyrme potentials have shown a reasonable compatibility for the longitudinal form factor calculations for all q values, and most cases were studied.

The OBDMs obtained from the USDA are appropriate to calculate the transverse form factors using the OXBASH and CPM3Y codes. This is due to the good agreement with the available experimental data for the excitation to the $J = 7/2^+_1$ state in ^{25}Mg. The theoretical results are discrepant with the experimental data for the transverse form factors observed in the transition to the $J = 9/2^+_1$ state. The interesting point in the calculations of the mixed multipolarity transverse form factors in the above cases is the sensitivity of $M5$ to the experimental data.

We found that the effective charges and effective g factors are necessary to describe the core-polarization effects in the OXBASH code calculations. The new effective charges ($e_p = 1.36$ and $e_n = 0.45$) and g factors : $g_s(p) = 5.0$, $g_s(n) = -3.5$, $g_l(p) = 1.175$, and $g_l(n) = -0.106$ [22] are appropriate to show results close to the experimental values for the $M1$, $E2$, and $M3$ transitions. On the other hand, the effective charges $e_p = 1.5$ and $e_n = 0.5$ are the appropriate values that can be used with $E4$ and the free-nucleon g factors with $M5$. We have found in this paper that $g_s(n) = -5.5$ is the appropriate coefficient to estimate the $M5$ transverse form factors from the experimental data for the transition to the $J = 9/2^+_1$ state.

For the elastic magnetic electron-scattering form factors, it has been found that the harmonic-oscillator potential gives the best agreement for the overall shape by decreasing the size parameter by 10% from the b_{rms} value. The $g_s(n) = -3.7$ showed significant effects to give more acceptable results for the multipolarity transverse elastic form factors.

Use of the effective charges and gyromagnetic ratios as calibration parameters appears to be a handicap of the shell-model calculations by using the OXBASH code. This conclusion points to the urgent need to find an approach by which the -factor values can be assigned to the different transitions and configurations in the target model space.

ACKNOWLEDGMENTS

We thank the University of Malaya, the University of Kerbala, and the University of Samarra for supporting this work. A. A. Al-Sammarraie wishes to thank the Islamic Development Bank (IDB) for supporting this work under Grant No. 600014283. A. A. Al-Sammarraie, N. Yusof, and H. A. Kassim acknowledge support for this work through the University of Malaya Postgraduate Research Grant No. PV089/2011A. N. Yusof and H. A. Kassim also acknowledge support from the University of Malaya Research Grant Programmes (Grants No. UMRG RP006C-13AFR and No. UMRG RP012D-13AFR). We acknowledge the help of Prof. D. Bradley and A. Cristini for proofreading this paper and for giving some constructive comments.

[1] R. Longland, C. Iliadis, and A. I. Karakas, Phys. Rev. C **85**, 065809 (2012).
[2] C. Massimi *et al.*, Phys. Rev. C **85**, 044615 (2012).
[3] R. Longland, C. Iliadis, G. Rusev, A. P. Tonchev, R. J. de Boer, J. Görres, and M. Wiescher, Phys. Rev. C **80**, 055803 (2009).
[4] B. Limata *et al.* (LUNA Collaboration), Phys. Rev. C **82**, 015801 (2010).
[5] M. Isaka, M. Kimura, A. Doté, and A. Ohnishi, Phys. Rev. C **87**, 021304(R) (2013).
[6] M. Isaka, M. Kimura, A. Doté, and A. Ohnishi, Nucl. Phys. A **914**, 189 (2013).
[7] M. Isaka, H. Homma, M. Kimura, A. Doté, and A. Ohnishi, Phys. Rev. C **85**, 034303 (2012).
[8] B. A. Brown, A. Etchegoyen, W. D. Rae, N. S. Godwin, W. A. Richter, C. H. Zimmerman, W. E. Ormand, and J. S. Winfield, MSU-NSCL Report No. 524, 1985 (unpublished).
[9] E. Caurier and F. Nowacki, Acta Phys. Pol., B **30**, 705 (1999).
[10] B. A. Brown and W. D. Rae, NuShell@MSU, MSU-NSCL report, 2007 (unpublished).
[11] B. A. Brown and W. D. Rae, http://www.nscl.msu.edu/_brown/resources/resources.html.
[12] B. H. Wildenthal, Prog. Part. Nucl. Phys. **11**, 5 (1984).
[13] B. A. Brown and W. A. Richter, Phys. Rev. C **74**, 034315 (2006).
[14] W. A. Richter and B. A. Brown, Phys. Rev. C **80**, 034301 (2009).
[15] G. Bertsch, J. Borysowicz, H. McManus, and W. G. Love, Nucl. Phys. A **284**, 399 (1977).
[16] K. S. Jassim, A. A. Al-Sammarrae, F. I. Sharrad, and H. A. Kassim, Phys. Rev. C **89**, 014304 (2014).
[17] A. A. Al-Sammarrae, F. I. Sharrad, A. A. Aziz, N. Yusof, and H. A. Kassim, Eur. Phys. J. Plus **129**, 125 (2014).
[18] B. A. Brown, *Lecture Notes in Nuclear Structure Physics* (National Superconducting Cyclotron Laboratory and Department of Physics and Astronomy Michigan State University, E. Lansing, MI 48824, 2011).
[19] B. A. Brown, B. H. Wildenthal, C. F. Williamson, F. N. Rad, S. Kowalski, H. Crannell, and J. T. O'Brien, Phys. Rev. C **32**, 1127 (1985).
[20] B. A. Brown, Phys. Rev. C **58**, 220 (1998).
[21] H. Chandra and G. Sauer, Phys. Rev. C **13**, 245 (1976).
[22] W. A. Richter, S. Mkhize, and B. A. Brown, Phys. Rev. C **78**, 064302 (2008).
[23] http://www.nndc.bnl.gov/chart/getENSDFDatasets.jsp.
[24] R. B. Firestone, Nucl. Data Sheets **110**, 1691 (2009).
[25] E. W. Lees, C. S. Curran, T. E. Drake, W. A. Gillespie, A. Johnston, and R. P. Singhal, J. Phys. G: Nucl. Phys. **2**, 341 (1976).
[26] B. A. Brown, G. Shen, G. C. Hillhouse, J. Meng, and A. Trzcinska, Phys. Rev. C **76**, 034305 (2007).
[27] E. W. Lees, C. S. Curran, S. W. Brian, W. A. Gillespie, A. Johnston and R. P. Singhal, J. Phys. G: Nucl. Phys. **1**, L13 (1975).
[28] J. R. Marinelli and J. R. Moreira, Phys. Rev. C **45**, 1556 (1992).
[29] H. Euteneuer *et al.*, Phys. Rev. C **16**, 1703 (1977).
[30] R. C. York and G. A. Peterson, Phys. Rev. C **19**, 574 (1979).
[31] T. W. Donnelly and I. Sick, Rev. Mod. Phys. **56**, 461 (1984).
[32] R. P. Singhal, A. Watt, and R. R. Whitehead, J. Phys. G: Nucl. Phys. **8**, 1059 (1982).
[33] R. A. Radhi, N. T. Khalafb, and A. A. Najimb, Nucl. Phys. A **724**, 333 (2003).